A mechanical criterion for Lüders-type deformation of polycrystalline NiTi

Yingchao Li[1], Bashir S. Shariat[1], Hong Yang[1], Satyajit Sarkar[1], Junsong Zhang[2], Yunzhi Wang[3], Denis Favier[4] and Yinong Liu[1*]

[1] Department of Mechanical Engineering, The University of Western Australia, Perth, WA 6009 Australia

[2] State Key Laboratory of Metastable Materials Science and Technology, Yanshan University, Qinhuangdao, Hebei 066004, China

[3] Department of Materials Science and Engineering, The Ohio State University, Columbus, OH 43210, United States

[4] Grenoble Alpes University, CNRS, Grenoble INP, TIMC-IMAG, F-38000 Grenoble, France

Abstract

NiTi shape memory alloys are known to exhibit a Lüders-type deformation behaviour associated with its stress-induced martensitic transformation. Such phase-transformation-caused Lüders deformation presents a different metallurgical mechanism to the dislocation-related Lüders deformation of mild steels. To explain this phenomenon, many hypotheses have been proposed in the literature. However, all these explanations seem to contradict some experimental evidence in one way or another. In this work, a new explanation for the occurrence of the Lüders-type deformation in NiTi is proposed and a model is derived based on the criterion of conservation of sample length changes produced by the stress-induced transformation, the crosshead movement of the testing machine and the elastic contraction. The model is verified by tensile experiment and digital image correlation measurement. The new model is able to describe the upper-lower yielding phenomenon and the plateau stress of the Lüders-type deformation behaviour.

Keywords: NiTi; Shape memory alloy; Martensitic phase transformation; pseudoelasticity; Lüders deformation.

1. Introduction

NiTi shape memory alloys (SMAs) are known to exhibit a Lüders-type deformation behaviour [1, 2], analogous to the Lüders deformation behaviour of mild steels [3]. The Lüders-type deformation in NiTi occurs during stress-induced martensitic transformation [4] or martensite reorientation [5], and for both the forward B2→B19' transformation upon loading and the reverse B19'→B2 transformation upon unloading [1]. The Lüders-type deformation has been observed to occur with an upper-lower yielding followed by a stress plateau with a strain span of typically 5~7% [6]. Such upper-lower yielding behaviour presents a typical situation of mechanical instability. Similar Lüders-type deformation behaviour has also been observed for stress-induced martensitic transformations in other alloy systems, such as NiFeGa (B2→10M→14M→L_{10} phase transformations) [7], CuZnAl (β→18R→6R) [8, 9] and FeMnNiAl (BCC→FCC) [10].

The Lüders-type deformation behaviour of NiTi has been observed to occur only in tension, and not in compression [11, 12], shear [11, 13], or biaxial tension [14]. Some studies reported the observation of strain localisation in simple shear [15] and torsion of thin wall tubes [16] and wires [17], but in all these cases the stress response increases monotonically with strain without the signature upper-lower yielding and the stress plateau of the Lüders deformation. In bending mode, the localized Lüders deformation appears in the tension side but not in the compression side [12]. In this regard, the Lüders-type deformation behaviour is a general phenomenon for stress-induced martensitic transformations and yet appears to be a special occurrence only to some specific mechanical conditions such as tension.

The Lüders deformation of NiTi has also been studied by various means in addition to mechanical testing. Video cameras [1, 18-20], infrared cameras [1, 21-24] and digital image correlation (DIC) technique [12, 15, 23, 25-28] have been used to observe the macroscopic behaviour of Lüders bands *in situ* during mechanical testing. Synchrotron X-ray diffraction [29-32], neutron diffraction [33] and electron backscatter diffraction (EBSD) [34] techniques have also been used to elucidate the phase transformation and microscopic metallurgical processes of the Lüders-type deformation. Transmission electron microscopic (TEM) examination has been carried out to study the detwinning process of martensite variants during Lüders-type deformation [35].

From these experiments, a broad empirical knowledge base of the Lüders-type deformation of NiTi has been established. Among the many characteristics of the Lüders-type deformation in NiTi, the following needs specific mentioning here. The Lüders-type deformation initiates by the sudden appearance of a narrow and localized strain band and proceeds by its propagation through the length of the sample over a stress plateau. The initiation of the band is associated with a stress drop, as commonly observed. Associated with the stress drop is an elastic strain reduction of the austenite part outside the newly formed Lüders band, as reported by Elibol and Wagner [25] and later by Shariat et al. [26]. During the propagation of the Lüders band, the strain inside the band remains relatively constant at a high value corresponding to the end of the global stress plateau whereas the strain outside the band also remains constant at a low value corresponding to the beginning of the stress plateau [4, 5, 23]. Upon the arrival of the Lüders band, the local strain increases rapidly from the low level to the high level [15, 23, 29, 32]. Shariat et al. conducted a DIC measurement and reported that the local strain rates at the initiation and during the propagation of a Lüders band are orders of magnitude higher than the nominal strain rate applied by the testing machine [26].

The martensitic transformation associated the Lüders-type deformation in shape memory alloys represents clearly a different metallurgical process from the dislocation-related Lüders deformation of mild steels [36, 37]. This requires a new understanding of the mechanism of the phenomenon. Despite the many studies, most of the published work in the literature focus on the characterisation of the phenomenon and only a few have devoted their attention to explaining the underlying mechanisms of the phenomenon. Miyazaki et al. first reported the Lüders-type deformation in NiTi and attributed the phenomenon to the effect of local stress concentrations at grain boundaries in the small-grain matrix of the alloy used [2]. This may support the self-catalytic nature of the martensitic transformation and thus the strain localisation, but clearly cannot differentiate between tension and compression/shear deformation modes. Shaw and Kyriakides [1] attributed the phenomenon to a higher stress required for martensitic transformation nucleation than that for martensite growth, in analogy to the phenomenon of nucleation supercooling for solidification. This explanation is challenged by a few considerations. For example, the Lüders-type deformation also occurs during stress-induced martensite reorientation, where no phase transformation (thus nucleation) is involved. For stress-induced transformations, the Lüders-type deformation is not observed in shear or compression [11, 38] or in biaxial tension [14] where martensite nucleation is required for the transformation. In addition, when a Lüders band propagates through a polycrystalline

matrix, concurrent nucleation and growth of martensite occur in every grain continuously throughout the propagation of the band from one end of the sample to the other. In this regard, this explanation is also unsupported.

Mao et al. used EBSD method to characterise the Schmid factors of various martensite variants in a polycrystalline NiTi and calculated their critical resolved shear stresses for stress-induced transformation. They compared these critical resolved shear stresses between tension and compression and explained the absence of Lüders deformation in compression on the basis of these differences [34]. In this work, the occurrence of Lüders deformation in tension is attributed to the self-catalytic effect of martensite, i.e., the stress field caused by the formation of one martensite variant in one grain triggers the formation of more martensite variants in an avalanche manner in the surrounding austenite grains. This will lead to a continuously radiating and expanding transformation region, as opposed to disconnected pockets, but how it is in the form of a band is not explained [34]. Sittner et al. [6] took a micromechanics modelling approach and provided a similar explanation for the tension-compression disparity for the occurrence of Lüders deformation in polycrystalline NiTi. Their modelling suggests that a unique partitioning of stresses, strains, and phase fractions among grains for textured polycrystalline NiTi exists under tension that allows it to deform via stress-induced martensitic transformation with very small deformation modulus over the stress plateau (often on an engineering stress-strain curve), thus favourable for a localised band deformation. Such partitioning does not occur in compression. Whereas a very low (and positive) deformation modulus over the apparent stress plateau for the stress-induced transformation may be favourable for a localized deformation, it does not present a strain softening (negative modulus) or a mechanical instability condition for an upper-lower yielding, which is essential for a Lüders deformation behaviour.

To overcome this conundrum, Hallai and Kyriakides [39] conducted a carefully designed comparative experiment using sandwiched steel-NiTi-steel and steel-steel-steel plate samples and derived a “natural” mechanical behaviour of stress-induced martensitic transformation of NiTi when strain localization is prevented from occurring (by the steel casing). This behaviour features a continuously decreasing stress, i.e., a continuous strain softening, over the course of the transformation in the sample. Such behaviour has enabled several successful finite element simulations of the Lüders-type deformation of NiTi samples [40-43]. However, neither the original work nor the later works have offered a metallurgical justification of such a behaviour,

i.e., why a stress-induced transformation will proceed with a progressively decreasing global stress. In summary, to date, a credible explanation of the mechanism of the occurrence of the Lüders deformation in NiTi is still absent.

In this work, we propose a new explanation for the occurrence of the Lüders-type deformation in NiTi based on the consideration of the mismatch between the fast speed of stress-induced martensitic transformation and the slow speed of deformation applied by the testing machine. The local strain rate of Lüders deformation in NiTi has been measured to be more than two orders of magnitude higher than the global strain rate applied by the testing machine [26]. Such large discrepancy between the two must have direct impact on the deformation behaviour of the alloy in tension. This paper presents the argument, the mathematical formulation, and the experimental verification of this mechanism for the occurrence of Lüders-type deformation in NiTi.

2. Experimental method

A commercial polycrystalline Ti-50.9at.%Ni sheet from Memry Corp. was used in this study. The sheet was 0.52 mm in thickness. The transformation behaviour of the as-received alloy was measured by differential scanning calorimetry (DSC) using a TA Instrument Discovery DSC 25 unit with a heating/cooling rate of 10 K/min.

Dog-bone shaped tensile samples (Fig. 1) were fabricated by wire cutting using an electrical discharge machine (EDM). The samples have a gauge section of 2.5×30 mm. Tensile testing was conducted using a WDT-10 universal mechanical testing machine at 28 °C (±0.5 °C) in an air-conditioned environment. A slow nominal strain rate of 1×10^{-4} s^{-1} was used to minimize the heating effect caused by the release of latent heat during the stress-induced martensitic transformation.

Digital image correlation (DIC) method was used to measure the strain fields on the surface of the tensile samples. The camera used was Sony α7R IV with 60.2 megapixels in a 9504×6336-pixel format. This gives a camera resolution of 3.76 μm on the sensor and 5.25 μm resolution on the sample on the image of 50×28 mm in dimension. This also implies a strain measurement resolution of 0.0175%. DIC analysis was conducted using the GOM Correlate Pro software. For this analysis, a grid size of 35 μm was used, which yielded

reliable data for local strain measurement. Images were captured at 1 Hz frequency.

3. Theoretical formulation of Lüders deformation mechanism in NiTi

3.1 The hypothesis

It is a common and fundamental knowledge that martensitic transformation occurs locally at a speed close to that of sound in the alloy [44]. This is due to the need to transmit the large lattice distortion strains through the matrix to a free surface or an internal interface so to be accommodated. The speed of this transmission is the speed of the mechanical waves of atoms in the lattice. Experimentally, the martensitic transformation in a Fe-29.5Ni alloy has been measured to propagate at a speed of ~1×10^6 mm/s, corresponding to roughly 1/3 of the speed of sound in the alloy [45]. The same behaviour has also been observed under high-speed camera on a NiTi thin-wall tube as the sudden formation of a transformation band, of which the interface front velocity was estimated to be up to 2×10^3 mm/s [19]. This is an intrinsic nature of the martensitic transformation. Recently, Shariat et al. used DIC technique to measure the local strain rates of Lüders deformation of a polycrystalline NiTi in tension and determined a local strain rate of 223×10^{-4} s^{-1} for the nucleation of a Lüders band [26], which is 223 times of the global strain rate applied by the testing machine, or corresponding to a sample elongation speed several times higher than the crosshead movement speed. This implies that the testing device is unable to provide the necessary elongation required by the formation of the Lüders band. In other words, a Lüders band cannot form unless additional elongation is provided to it. With these thoughts, we hypothesize that elastic contraction of the sample outside the band is the source of this "additional" elongation required for the formation of the Lüders band. This is consistent with the observed stress drop [1] and elastic strain drop [25] observed at the initiation of a Lüders band. In addition, it is also known that elastic deformation occurs by the same mechanism of lattice waves of atoms, i.e., also at the speed of sound in the solid, thus has the intrinsic ability to match in speed with the martensitic transformation.

In this hypothesis, the occurrence of martensitic-transformation-associated Lüders-type deformation must have four essential conditions:

(1) The martensite must form into a continuous band and the band must reach the free surface of the sample due to the need to accommodate (relax) the large lattice strain

energy of the transformation.

It is known that the martensitic transformation is associated with a lattice distortion of a finite lattice strain [46]. Due to the diffusionless nature of the transformation [47], the lattice distortion of the unit cell manifests as a shape change of a martensite (M) crystal relative to the austenite (A) it replaces. In a thermally-induced martensitic transformation, these local shape changes of the martensite crystals are self-accommodated in variants of different orientations [48]. In a stress-induced martensitic transformation, the selection of variants is dictated by the need to produce a maximum strain in the loading direction, thus there is no freedom for self-accommodation (in fact, there is still a secondary self-accommodation among the variants in the lateral directions to maintain a nil lateral shape distortion and loading axis alignment). In this case, the formation of one martensite in one grain with an elongated dimension relieves itself immediately from bearing the load, thus redistributing the load to the adjacent grains in parallel to the loading axis and preferably triggering the transformation there. This has been referred to as the self-catalytic or the avalanche effect of martensitic transformations. It dictates the martensite to form into a continuous region (band), as opposed to scattered and disconnected islands, until a free surface is reached, so to maintain the matrix continuity and to avoid excessively large and prohibitive internal elastic lattice distortions. From a mechanics viewpoint, in tension, this localized martensite region forms into a narrow band across the entire cross-section of the sample in series configuration with the untransformed part of the sample in the loading direction (same for compression). In the case of simple shear, the band runs across the sample in parallel configuration with the shear direction.

(2) The localized transformation band (Lüders band) must have a finite length (Note: this refers to the dimension of the band along the gauge length of a tensile sample, or the direction of the tensile load. This dimension has also sometimes been intuitively referred to as the width of the band when the band is newly formed and is narrow and thin. In this discussion, we use “length” so to be mathematically more consistent with the mechanics of the situation) in a polycrystalline matrix, so to be able to accommodate sufficient number of grains for coordination among the strain tensors of the variants in neighbouring grains across their boundaries.

(3) The localized transformation band must have a discrete strain output. This is apparently true considering the transformation crystallography and it is a collective manifestation of the crystallographic changes of the martensite variants in a polycrystalline matrix.

(4) The local strain rate (in the direction of loading) of this localized transformation band, which is a collective manifestation of the speed of the martensitic transformation, is high, in fact, much higher than the nominal strain rate applied by the testing machine.

The combination of the four conditions above produces a fast elongation rate by the sample upon the occurrence of the Lüders-type deformation. This implies that the testing machine must provide such fast elongation rate to allow the Lüders-type deformation to occur, i.e., meeting this elongation rate is an essential condition for Lüders-type deformation.

3.2 Mathematical model

Based on this hypothesis, a mathematical model is developed based on the criterion of sample length change conservation in real time among three contributions: sample length change (elongation) produced by the formation (or expansion) of a Lüders band (δ_L), sample length change (elongation) caused by the crosshead displacement of the testing machine (δ_m), and the sample length change (reduction as a negative value) by the elastic contraction of the rest of the sample (δ_{el}). This relationship can be expressed for any time interval between t_I and t_{II} during the deformation as:

$$\delta_m = \delta_L + \delta_{el} \tag{1}$$

The same may also be expressed in differential form, i.e.,

$$\dot{\delta}_m = \dot{\delta}_L + \dot{\delta}_{el} \tag{2}$$

which states that the rate of sample length elongation applied by the testing machine equals the sum of those provided by the activity (formation or propagation) of the Lüders band and the change of elastic strain in the sample.

To derive the model, the following variables are defined:

ε_A is the local strain of the austenite, and ε_L is the local strain inside the Lüders band.

ε_t is the global strain over the full gauge length based on direct DIC measurement at momont t (i.e., it is a function of time t).

V_m is the machine crosshead movement speed, which can be obtained from the experiment.

$\lambda_{L,A}$ is the length of the original austenite corresponding to the *active* length of the Lüders band (λ_L). The active length of a Lüders band is the full length of the band during its initiation and is the front transition zone of a band during its propagation. $\lambda_{L,A}$ can be measured from the experiment, but cannot be controlled.

$l_{L,A,\mathrm{t}}$ is the length of the original austenite that has transformed to the Lüders band of length $l_{L,\mathrm{t}}$. It is a function (variable) of time t (since the Lüders band grows with time), i.e., it is an instantaneous length at t. It is also the length of the original austenite at the stress-free state (no elastic strain). It can be computed as $l_{L,A,\mathrm{t}} = \frac{l_{L,\mathrm{t}}}{(1+\varepsilon_{L,\mathrm{t}})}$, where $l_{L,\mathrm{t}}$ can be measured from the experiment and controlled during the experiment.

L_0 is the initial gauge length of the sample at the stress-free state, which can be obtained from the experiment. Thus $(L_0 - \lambda_{L,A})$ is the original length of the section of the sample excluding the active section of the Lüders band, which participates in elastic contraction during Lüders deformation.

$\dot{\varepsilon}_L$ is the local strain rate within the newly formed Lüders band, which can be measured from the experiment, but cannot be controlled.

$\dot{\varepsilon}_{el}$ is the strain rate of the elastic contraction of the sample in the section excluding $\lambda_{L,A}$, which can be measured from the experiment, but cannot be pre-determined or controlled.

Some notes should also be added on the notation of the parameters:

(i) <u>*Capital-case symbols*</u> are used for testing constants (such as sample initial gauge length L_0).

(ii) <u>*Lower-case symbols*</u> are used to express instantaneous values (such as length of the Lüders band l_L and the length of the austenite section that transforms into a new Lüders band $l_{L,A}$).

(iii) <u>*Numeral subscripts*</u> are used to indicate global strains at different stages of the deformation process (such as ε_1 and ε_2 for the global strains at point 1 and point 2 on the stress strain curve, respectively).

(iv) *Roman numeral subscripts* are used to designate a specific point in time.

(v) *Capital letter subscripts* are used to indicate local strains at specific locations of the sample along the length (such as ε_L for the instantaneous local strain inside a Lüders band and ε_A for the local strain in the austenite region of the sample outside the Lüders band), considering non-uniformity of the local strains along the length of the sample due to the Lüders deformation behaviour.

(vi) Three different strain terms are used in this discussion, including (i) nominal strain, (ii) global strain and (iii) local strain. These are all engineering strains. Consequently, there are three corresponding strain rates. The nominal strain refers to the crosshead displacement divided by the original gauge length of the sample. In the case of localized heterogeneous deformation, this strain does not represent any actual strain in the sample. The global strain is the strain measured by DIC over full gauge length of the sample. This is in principle the same as the nominal strain, but more practically accurate without the side effects of the shoulders of the dog-bone shaped sample and the griping etc. The global strain is used in the model analysis, whereas the nominal strain is used only in discussion to express the argument on the effect of the machine speed. The local strain is DIC measured strain at a local location. Considering that we use a grid size of 35 □m for DIC data processing, the local strain is an average strain within that dimension.

4. Model development

4.1 Characterisation of Lüders-type deformation

To develop the analytical solution of the conceptual model expressed in Eqs. (1) and (2), some parameters need to be determined experimentally. Fig. 1 shows the DIC field maps of the axial strain ε_x of a sample at two different points in time during the pseudoelastic Lüders deformation. Fig. 1(a) corresponds to the time when the Lüders band was just initiated. Fig. 1(b) shows the Lüders band in the propagation stage. Some parameters defined above are indicated in the figure, including the current gauge length of the sample $(1+\varepsilon_t)L_0$ at time t, the current length of the Lüders band l_L at time t and the active length of the Lüders band $\lambda_{L,A}(1+\varepsilon_t)$ (where $\lambda_{L,A}$is the length of the original austenite corresponding to the active length of the Lüders band. It is noted that the active length of a Lüders band is the whole length of the band $l_L = \lambda_{L,A}(1+\varepsilon_L)$ during the initiation stage of the band, but only the moving front edge(s) of the Lüders band during its propagation. In addition, two

observation points on the sample for local strain analysis are also indicated in the figure. Point P1 is at the initiation site of the Lüders band and P2 is far away in the austenite region.

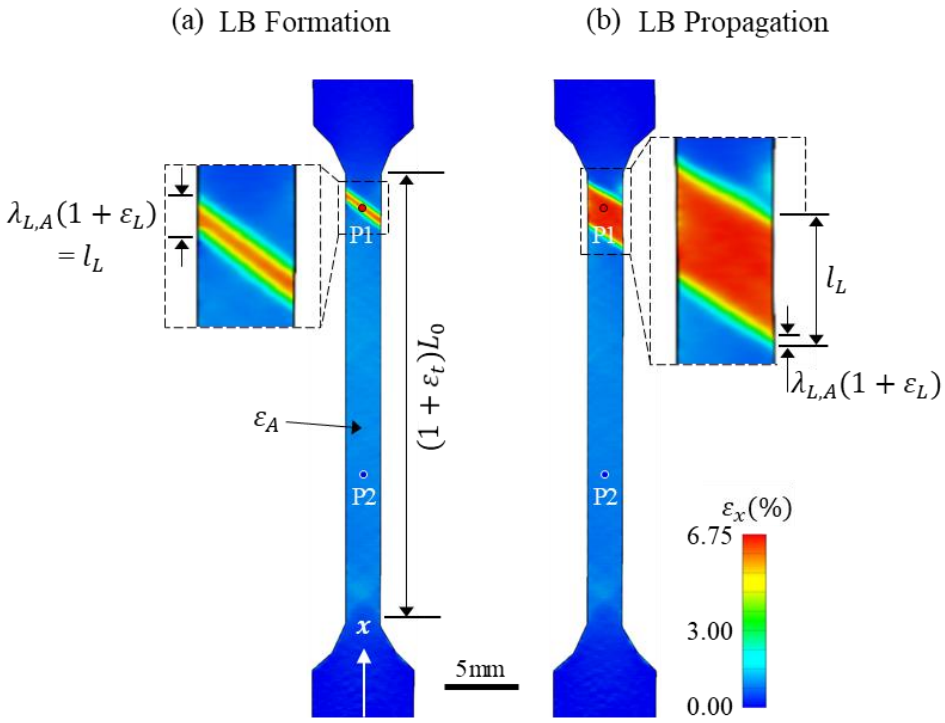

Figure 1. DIC ε_x strain maps of a sample at two different stages of the Lüders-type pseudoelastic tensile deformation. (a) Initiation of a Lüders band. (b) Lüders band propagation stage.

Fig. 2 shows the Lüders-type deformation behaviour induced by tension of a Ti-50.9at.%Ni alloy. Fig. 2(a) shows a pseudoelastic stress-strain curve of a 30 mm gauge length dog-bone shaped plate sample deformed under a global strain rate of 1×10^{-4} s^{-1}. The sample showed a clear Lüders deformation mode. Fig. 2(b) is an enlarged view of the stress drop at the onset of the Lüders deformation, as indicated by the box in (a). Point 1 is the peak point on the global stress-strain curve before the stress-drop, point 4 is the end of the stress drop (the beginning of the stress plateau), and point 7 is the end point of the stress plateau. Based on the stress evolution, the Lüders-type deformation behaviour may be divided in two stages: (i) the formation of a Lüders band, which is associated with a continuous stress drop, corresponding to stage 1-4, and (ii) the propagation of the Lüders band at a constant stress, which corresponds to stage 4-7.

Fig. 2(c) shows the strain-time curves for the same test, including the global strain (the black

curve) and the two local strains at points P1 and P2 on the sample (shown in Fig. 1) as determined by DIC method. It is seen that the local strains at both P1 and P2 increased linearly with time, apparently corresponding to the elastic deformation of the sample, until 190 s when the P1 local strain increased suddenly, demonstrating the burst formation of the Lüders band. The local strain rate at P1 reached 223×10^{-4} s^{-1}, which was 223 times higher than the applied global strain rate (1×10^{-4} s^{-1}). The local strain at P2 remained relatively unchanged until ~520 s when it also increased suddenly, signalling the arrival of the Lüders band front. The local strain rate at P2 when the Lüders band front swept through reached 26×10^{-4} s^{-1}, which was 26 times higher than the applied global strain rate. It is also to be noted that the magnitude of strain increases at P1 and P2 is the same, representing the strain of the Lüders band. This strain rise corresponds to $(\varepsilon_7 - \varepsilon_1)$ in global strain on the stress-strain curve.

Fig. 2(d) is an enlarged view of the strain curves in the section identified by the small box d in (c), which corresponds to the section of the stress drop seen in (b). The numerals indicated in (d) correspond to those in (b) in real time. It is evident that corresponding to the progressive stress drop, the strain at P2, which represents the elastic strain in the austenite region outside the newly formed Lüders band, decreased continuously within the same time period, as expected based on Hooke's law.

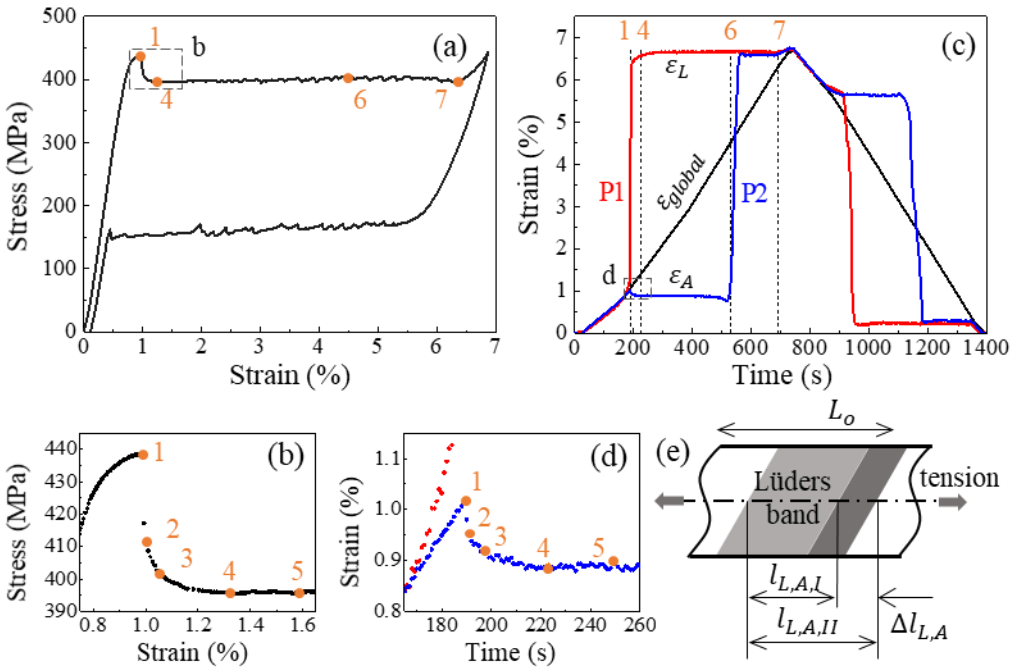

Figure 2. The phenomenon of Lüders-type deformation of NiTi. (a) A tensile pseudoelastic stress-strain curve of a 30 mm long NiTi dog-bone shaped sample deforming in Lüders band

mode. (b) An enlarged view of the area in the dashed box in (a) showing details of the stress drop at the onset of the Lüders deformation. (c) Time evolution of local strains at two locations (P1 and P2 indicated in Fig. 1) along the length of the sample and the DIC-measured global strain (average strain) over the full gauge length during the pseudoelastic deformation cycle. (d) An enlarged view of the area in the dashed box in (c) showing details of the strain relaxation of the austenite at the onset of the Lüders deformation. In (b) and (d), points 2, 3, 4, and 5 represent the stress and strain states at 2 s, 8 s, 29 s and 60 s after point 1. (e) Schematic of the expansion of the Lüders band from one point in time to the next.

4.2 Analytical solution of the model

To derive the solutions of the three terms in the model expressed in Eq. (1), let us examine the sample length changes between any two points in time during the Lüders-type deformation process, i.e., from t_I to t_{II}. During this period, the crosshead displacement δ_m can be computed as:

$$\delta_m = L_0(\varepsilon_{II} - \varepsilon_I) = V_m t \tag{3}$$

where ε_I and ε_{II} are the global strains of the sample at t_I and t_{II} respectively, V_m is the speed of the movement of the crosshead of the testing machine, and t is the generic variable time. They are measured directly from the experiment.

To solve the second term δ_L (note: it is important to reiterate that this is not the change of the length of a Lüders band, but the sample elongation caused by the formation or expansion of a Lüders band), let us examine the change of $l_{L,A}$ from t_I to t_{II}, as schematically expressed in Fig. 2(e). Here $l_{L,A,t}$ represents the instantaneous length of the original austenite corresponding to the length of the Lüders band ($l_{L,t}$) at time t in the stress-free state, thus $l_{L,A,t} = \frac{l_{L,t}}{1+\varepsilon_{L,t}}$. At t_I, the Lüders band length is $l_{L,I}$ and the corresponding length of the original austenite is $l_{L,A,I}$, thus the sample elongation generated by this length of the Lüders band is $(\varepsilon_{L,I} - \varepsilon_{A,I})l_{L,A,I}$, where $\varepsilon_{L,I}$ is the local strain inside the Lüders band at t_I and $\varepsilon_{A,I}$ is the (elastic) strain of the austenite at t_I. Thus $(\varepsilon_{L,I} - \varepsilon_{A,I})$ expresses the strain increase of the Lüders band. Similarly, at t_{II}, the length of the Lüders band is $l_{L,II}$, and the corresponding sample elongation now is $(\varepsilon_{L,II} - \varepsilon_{A,I})l_{L,A,II}$, where $\varepsilon_{L,II}$ is the strain inside the Lüders band at t_{II}. Therefore, the net sample elongation produced by the expansion of the Lüders band from t_I to t_{II} can be expressed as:

$$\delta_L = (\varepsilon_{L,II} - \varepsilon_{A,I}) l_{L,A,II} - (\varepsilon_{L,I} - \varepsilon_{A,I}) l_{L,A,I} \quad (4)$$

All the parameters in this equation, including $l_{L,A,I}$ ($l_{L,I}$), $l_{L,A,II}$ ($l_{L,II}$), $\varepsilon_{L,I}$, $\varepsilon_{L,II}$ and $\varepsilon_{A,I} = \varepsilon_1$, are determinable directly in experiment.

The third term is the elastic contraction of the sample, as seen in Fig. 2(d). This elastic contraction occurs to the entire length of the sample, except the active part of the Lüders band (λ_L with the corresponding length of the original austenite being $\lambda_{L,A}$) which transforms and produces the δ_L discussed above, i.e., the sample length that participates in elastic contraction is $(L_0 - \lambda_{L,A})$. Thus, the elastic contraction can be expressed as:

$$\delta_{el} = (\varepsilon_{el,II} - \varepsilon_{el,I})(L_0 - \lambda_{L,A}) = \Delta\varepsilon_{el}(L_0 - \lambda_{L,A}) \quad (5)$$

In this equation, $\varepsilon_{el,I}$ and $\varepsilon_{el,II}$ represent the average (elastic) strains of the length of the sample excluding the active region of the transformation $\lambda_{L,A}$. Apparently, here the elastic moduli of the austenite (A) and the martensite (M) are assumed the same [49]. Thus, $\Delta\varepsilon_{el} = \varepsilon_{el,II} - \varepsilon_{el,I}$ represents the elastic strain change (contraction is designated negative) of the sample length $(L_0 - \lambda_{L,A})$. The active length $\lambda_{L,A}$ evolves with time during the formation of the Lüders band and remains constant during its propagation [26]. It is believed to be determined or influenced by three intrinsic factors, including (1) the transformation crystallography, which determines the discrete strain jump between the two phases that the transition zone needs to accommodate, (2) metallurgical condition of the matrix (e.g., grain size, texture), which needs to rally and organize sufficient grains (martensite variants) to form a reasonably continuous strain field in the context of continuum mechanics to accommodate the strain transition, and (3) the cross-section geometry of the sample (e.g., wire, rod, thin plate or thick plate) which a Lüders band transition zone has to penetrate through. It is also clear that all parameters required in Eq. (5) can be determined experimentally.

Substituting Eqs. (3), (4) and (5) into Eq. (1) and solving the new equation for the elastic strain contraction $\Delta\varepsilon_{el}$ gives:

$$\Delta\varepsilon_{el} = \frac{(1+\varepsilon_{L,I})(1+\varepsilon_{L,II})(\varepsilon_{II}-\varepsilon_I)L_0 - (1+\varepsilon_{L,I})(\varepsilon_{L,II}-\varepsilon_{A,I})l_{L,II} + (1+\varepsilon_{L,II})(\varepsilon_{L,I}-\varepsilon_{A,I})l_{L,I}}{(1+\varepsilon_{L,I})(1+\varepsilon_{L,II})(L_0-\lambda_{L,A})} \quad (6)$$

Following the Hooke's law, the stress drop $\Delta\sigma$ from t_{I} to t_{II} can be determined as:

$$\Delta\sigma = E\Delta\varepsilon_{el} = E\frac{(1+\varepsilon_{L,I})(1+\varepsilon_{L,II})(\varepsilon_{II}-\varepsilon_I)L_0 - (1+\varepsilon_{L,I})(\varepsilon_{L,II}-\varepsilon_{A,I})l_{L,II} + (1+\varepsilon_{L,II})(\varepsilon_{L,I}-\varepsilon_{A,I})l_{L,I}}{(1+\varepsilon_{L,I})(1+\varepsilon_{L,II})(L_0-\lambda_{L,A})} \quad (7)$$

where E is the apparent elastic modulus of the sample length $(L_0 - \lambda_{L,A})$, and in this analysis $E = E_M = E_A$.

For the parameters identified above, $\varepsilon_{L,I}$ and $\varepsilon_{L,II}$ are the instantaneous local strains of (inside) the Lüders band at t_I and t_{II}, $l_{L,I}$ and $l_{L,II}$ are the lengths of the Lüders band at t_I and t_{II}, and $\lambda_{L,A}$ is the original austenite length corresponding to the active length of sample during the Lüders deformation, i.e., the evolving length of the Lüders band during its formation or the active front of the Lüders band during its propagation. These parameters can be determined experimentally by local strain measurement (e.g., DIC). $\varepsilon_{A,I}$ is the local strain in the austenite section outside the Lüders band at t_I. ε_I and ε_{II} are the global strains at t_I and t_{II} respectively on the stress-strain curve. Thus $\varepsilon_{A,I}$, ε_I and ε_{II} can be determined by global stress-strain curve measurement. L_0 is the original gauge length of the sample, and V_m is the elongation speed of the testing machine. Both are setting parameters of the experiment, i.e., also available from the experiment.

In addition, from Eqs. (4) and (5), the rates of sample elongations produced by the Lüders band and by the elastic contraction can also be obtained by differentiating the equations against time. In this case, $\varepsilon_{A,I}$, $\varepsilon_{L,I}$ and $l_{L,A,I}$ are of the chosen time point t_I and thus function as known values for differentiation, whereas $\varepsilon_{L,II}$ and $l_{L,A,II}$ for t_{II} are the time variables for differentiation, thus:

$$\dot{\delta}_L = \dot{\varepsilon}_L l_{L,\mathrm{A}} + (\varepsilon_{L,II} - \varepsilon_{A,I})\dot{l}_{L,A} \tag{8}$$

$$\dot{\delta}_{el} = \dot{\varepsilon}_{el}(L_0 - \lambda_{L,A}) - \Delta\varepsilon_{el}\dot{\lambda}_{L,A} \tag{9}$$

4.3 Formation and propagation of a Lüders band as defined by the model

Eqs. (6) and (7) are applicable to the entire Lüders-type deformation process. Depending on the values of $\Delta\varepsilon_{el}$ and $\Delta\sigma$, the entire process may be divided into two distinctive stages, i.e., the Lüders band formation stage and the propagation stage. The Lüders band propagation stage is defined as $\Delta\sigma = 0$ and $\Delta\varepsilon_{el} = 0$, which also implies $\dot{\varepsilon}_{el} = 0$. According to Eq. (9), therefore, $\dot{\delta}_{el} = 0$. Further, according to Eq. (2), $\dot{\delta}_m = \dot{\delta}_L$.

The Lüders band formation stage is characterized by $\Delta\sigma < 0$ and $\Delta\varepsilon_{el} < 0$. It commences

at point "1" and ends at point "4" as designated in Fig. 2(b). In this case, t_I corresponds to point "1" on the stress-strain curve, $l_{L,I} = 0$, $\varepsilon_{L,I} = \varepsilon_{A,I} = \varepsilon_1$ [5] (the sample is in full austenite state and the strain is uniform in the sample), and $\lambda_{L,A} = l_{L,A,II}$. Also substituting $l_{L,II} = (1 + \varepsilon_{L,II}) l_{\mathrm{L,A},II}$ for convenience of experimental measurement, Eqs. (6) and (7) are reduced to:

$$\Delta\varepsilon_{el} = \frac{(1+\varepsilon_{L,II})(\varepsilon_{II}-\varepsilon_1)L_0-(\varepsilon_{L,II}-\varepsilon_1)l_{L,II}}{(1+\varepsilon_{L,II})L_0-l_{L,II}} \tag{10}$$

$$\Delta\sigma = E\frac{(1+\varepsilon_{L,II})(\varepsilon_{II}-\varepsilon_1)L_0-(\varepsilon_{L,II}-\varepsilon_1)l_{L,II}}{(1+\varepsilon_{L,II})L_0-l_{L,II}} \tag{11}$$

When t_{II} corresponds to point "4" on the stress-strain curve, Eq. (12) expresses the full stress drop $\Delta\sigma_{full}$ of the Lüders-type deformation. In this case, $l_{L,II} = l_{L,4}$ and $\varepsilon_{II} = \varepsilon_4$. Parameter $\varepsilon_{L,II}$ is the strain within the Lüders band at point "4". Considering the Lüders-type deformation nature, $\varepsilon_{L,II} = \varepsilon_7$, where ε_7 is the global strain at the end of the stress plateau on the stress-strain curve seen in Fig. 2(a) [5]. Thus:

$$\Delta\sigma_{full} = E\frac{(1+\varepsilon_7)(\varepsilon_4-\varepsilon_1)L_0-(\varepsilon_7-\varepsilon_1)l_{L,4}}{(1+\varepsilon_7)L_0-l_{L,4}} \tag{12}$$

In this equation, ε_1, ε_4 and ε_7 are all directly measured from the global stress-strain curve of a conventional tensile mechanical testing, L_0 is the sample initial gauge length, and $l_{L,4}$ is length (dimension in the loading direction) of the Lüders band at point "4", which needs to be determined visually, e.g., using a visible camera, an infrared camera or by means of DIC technique. Based on Eq. (12), it can be recognized that the full stress drop $\Delta\sigma_{full}$ of the Lüders-type deformation is dependent on two parameters, in addition to the three characteristic strains mentioned above: sample initial gauge length L_0 and the length of the Lüders band l_L^* (which is $l_{L,4}$ re-denoted for generality) at its full birth prior to propagation. It is expected that l_L^* is dependent on the crystallography of the transformation, magnitude of the lattice distortion strain, grain size and texture of the austenite matrix, and the sample geometry.

5. Model Simulation of the stress-strain response of the Lüders-type deformation

5.1 Experimental data preparation

Fig. 3 shows a time resolved DIC strain analysis of the deformation process shown in Fig.

1(a). Fig. 3(a) plots the axial normal strain (ε_x) profiles along the central line of the sample at different times from point "1" to point "5" as indicated on the stress-strain curve seen in Fig. 2(b). Fig. 3(b) shows the ε_x strain field image of the sample as at the time corresponding to point "5". The emerging strain peak in the profiles indicates the formation of a Lüders band. It is seen that in the initial stage of the formation of the Lüders band both the peak strain and the length (width of the strain profile) of the Lüders band increased. During this stage, small changes also occurred to the austenite part outside the band. Fig. 3(c) shows an enlarged view of the progressive decrease of the strain of the austenite at time points "1-5". This corresponds to the strain-time shown in Fig. 2(d), which is measured at one observation point.

Fig. 3(d) plots the time evolutions of the peak strain (ε_L) and the length (l_L) (measured as the width of the strain profile at half height) of the Lüders band. It is seen that the strain rate ($\dot{\varepsilon}_L$) is the most rapid between points "1" and "2" (within 2 seconds), which is measured to be 0.0223 s^{-1}. This strain rate is 223 times of the applied global strain rate. This demonstrates the burst initiation of the Lüders band. This is followed by a continued growth of the peak strain inside the Lüders band to the maximum ($\varepsilon_{L,max} = 6.42\%$) at point 3. After this, further sample elongation is provided by the expansion of the length of the Lüders band, and not further increase of the peak strain inside the Lüders band. In this is regard, the Lüders-type deformation process may also be considered in two distinctive stages at point 3. It is also to be pointed out that prior to point "3", the active length of the Lüders band contributing to elongation is the full length of the band (full width of the strain profile), i.e., following the path of the red curve in (d). After point "3", the active length of the Lüders band becomes one moving front of the band (the second front is arrested by the end of the sample in this case), i.e., following the dashed red line in (d).

Using exponential curve fitting, the $l_L(t)$ and $\varepsilon_L(t)$ curves shown in Fig. 3(d) can be empirically expressed as:

$$l_L(t) = -0.58e^{-0.216t} + 0.057t + 1.111\ (mm) \quad (13)$$

$$\varepsilon_L(t) = -5.117e^{-0.902t} + 6.478\ (\%) \quad (14)$$

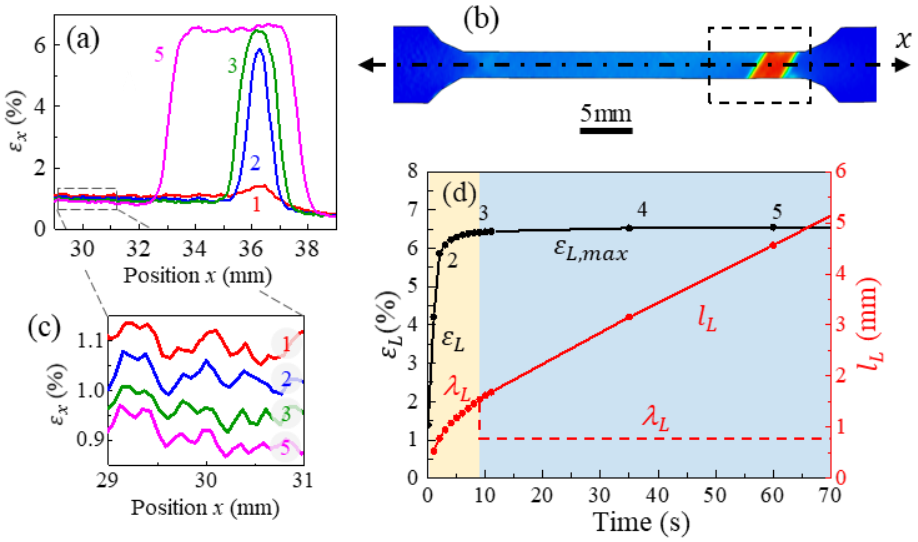

Figure 3. Time-resolved strain analysis of the initiation and propagation of a Lüders band based on DIC measurement. (a) Local strain profiles along the centre line of a sample at different times during Lüders band deformation. (b) DIC image of the axial strain ε_x map of the sample as at the time corresponding to point "5". The dashed box indicates the area of the ε_x profiles shown in (a). (c) Changes of the elastic strain of the austenite outside the Lüders band during its formation and propagation. (d) Evolutions of the length l_L and the peak strain ε_L of the Lüders band. The numerals correspond to those identified in Fig. 2.

5.2 Model simulation of the experimental data

Using the experimental data $l_L(t)$ and $\varepsilon_L(t)$ as expressed by Eq. (13) and (14), the Lüders deformation behaviour can be analysed. First let's examine the sample elongation produced by the Lüders band, which is described by Eq. (4). The Lüders deformation commences at point "1". At this point, t_I is set as 0 ($t_I = 0$), t_{II} is taken as the time variable t ($t_{II} = t$), $\varepsilon_{A,I} = \varepsilon_1$, $l_{L,A,I} = 0$, and given that $l_{L,A,t} = \frac{l_{L,t}}{1+\varepsilon_{L,t}}$, Eq. (4) becomes:

$$\delta_L(t) = (\varepsilon_{L,t} - \varepsilon_1)\frac{l_{L,t}}{1+\varepsilon_{L,t}} \tag{15}$$

Using the experimental data $l_L(t)$ and $\varepsilon_L(t)$ as expressed by Eq. (13) and (14) for $l_{L,t}$ and $\varepsilon_{L,t}$ respectively, $\delta_L(t)$ is computed as a function of time using Eq. (15) and plotted in Fig. 4(a). Using Eq. (3), $\delta_m(t)$ is also calculated as a function of time and plotted in the figure. Then $\delta_L(t) - \delta_m(t)$ is computed, as shown in the figure. It is seen that in the early stage of the Lüders deformation δ_L increased much faster than δ_m. This excess of elongation

($\delta_L - \delta_M$) is the cause of the elastic strain contraction, thus the stress drop, of the Lüders deformation. The raise of ($\delta_L - \delta_m$) slowed down gradually and reached a constant value at point "4", indicating that the elongation rate from the Lüders band equals that produced by the testing machine. This represents the stress plateau stage of the Lüders deformation.

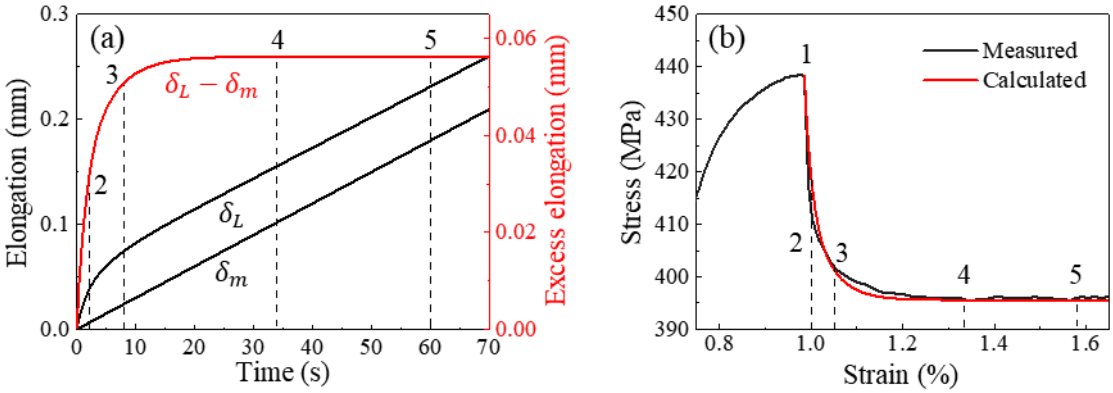

Figure 4. Model simulated tensile stress-strain behaviour of the Lüders-type deformation of NiTi. (a) Comparison between the sample elongation produced by the Lüders band δ_L and that provided by the testing machine δ_m. (b) Comparison of the experimentally measured and the model calculated stress-strain curves of the sample.

It is to be noted that at point "3", $\varepsilon_L(t)$ reached the maximum and the active Lüders band length λ_L reached the maximum (Fig. (3)) and at point "4", the magnitude of the stress drop $\Delta\sigma$ reached the maximum (Fig. 2). These two points represent two different characteristic points in time of the Lüders deformation process.

The stress-strain behaviour of the Lüders deformation (the section between point "1" and "7" on the stress-strain curve shown in Fig. 2(a)) can also be calculated by the model. The stress drop $\Delta\sigma$ is described by Eq. (7). As discussed above, when calculated from point "1", Eq. (7) is reduced to Eq. (11). Further, for the stage from point "1" to point "3", $\lambda_L = l_{L,II}$ (Fig. 3(d)), which is defined by Eq. (13), $\varepsilon_{L,II}$ is defined by Eq. (14), and with ε_1=1.0% as the global strain and σ_1=436 MPa at point "1" (both measured from the stress-strain curve shown in Fig. 2(a)), E=22 GPa being the apparent modulus of the austenite section as determined directly from the stress and strain measurements shown in Figs. 2(b) and (d), L_0=30 mm being the sample gauge length, and $\varepsilon_{II} = \varepsilon$ as the variable, then using Eq. (11) the stress drop $\Delta\sigma$ is calculated as a function of ε and $\sigma = \sigma_1 + \Delta\sigma$ as the stress is plotted

in Fig. 4(b).

For the section after point "3" to point "7", the Lüders band starts to expand on one front only, thus its active length λ_L remains unchanged as roughly half of the length at point "3", as expressed in Fig. 3(d). In this case, t_I represents point "3", and λ_L=0.7 mm as determined by DIC measurement (Figs. 1(b) and 3(d)), thus $\lambda_{L,A} = \frac{\lambda_L}{1+\varepsilon_{L,I}}$, $\varepsilon_{L,I}$=6.42% is the Lüders band strain at point 3 (Fig. 3(d)) (or it can also be calculated using Eq. (14)), $\varepsilon_{L,II}$ is the time function of ε_L given in Eq. (14), ε_I=1.05% is the global strain at point "3" (Fig. 2(b)), $\varepsilon_{A,I}$=0.92% is the elastic strain of the austenite section at point 3 (Fig. 2(d)), $l_{L,II}$ is the time function of l_L given in Eq.(13), $l_{L,I}$=1.55 mm is the length of the Lüders band at point "3" (Fig. 3(d)), and σ_3=401 MPa is the global stress at point "3" (Fig. 2(b)), then using Eq. (7) the stress drop $\Delta\sigma$ for the section after point "3" is calculated and $\sigma = \sigma_3 + \Delta\sigma$ as the stress is also plotted in Fig. 4(b), together with the actual experimental stress-strain curve. It is evident that the two curves match nearly perfect.

6. Interpretation of other empirical observations based on this model

6.1 Stress-induced martensitic transformation under other loading conditions than tension

As presented above, Lüders-type deformation in NiTi has been observed empirically to occur in tension and not in compression or shear. The model presented above needs to be cross-examined with regard to those experimental observations.

The model declares one criterion of sample elongation conservation among all contributions on real time, including machine crosshead movement, Lüders band deformation and elastic strain contraction. Whereas the overspeed of the elongation production by the Lüders band over the machine crosshead movement is the root course for the elastic strain contraction, the elastic strain contraction, which implies a stress relaxation, is the prerequisite condition of deformation softening for the occurrence of the Lüders-type localized deformation.

The amount (rate) of the elastic strain contraction δ_{el} required is determined by the speed of the elongation generated by the Lüders band formation $\dot{\delta}_L$, which in turn can be decomposed into three aspects: the strain increment $\Delta\varepsilon_L = (\varepsilon_L - \varepsilon_A)$ of the Lüders band, the speed of this strain increment $\dot{\varepsilon}_L$, and the initial (active) length of the Lüders band l_L (or λ_L) at its

sudden formation. On the other hand, the supply of a sufficient elastic strain contraction δ_{el} is dependent on the sample having a sufficient gauge length L_0 for a given $\Delta\varepsilon_{el}$, as per Eq. (5).

It has been considered that the absence of Lüders-type deformation in compression and shear is possibly caused by the generally short gauge length used in such tests. However, the following experimental evidence defies such a conclusion. Orgéas and Favier [11] conducted a comparative tension and compression test of identical typical "dog-bone" plate samples with narrow stripe gauge section of 40 mm in length (gauge section dimension 40×5.6×2.7 mm), using a specially designed constraint device to prevent compression buckling. This is probably the highest length to width/thickness aspect ratio used for compression testing in the literature. This sample did not exhibit Lüders-type deformation in compression. This experiment indicates that the absence of Lüders-type deformation in compression cannot be argued for the lack of sufficient sample gauge length.

Shear testing is another case where short sample "gauge length" is commonly used. For simple plate shear tests, the sample usually has a very narrow "gauge width" (which is effectively the length direction for Lüders band formation) and a large length parallel to the shear direction (which is effectively the width for Lüders band formation). This gives a very small aspect ratio well below 1 for the formation of a Lüders band [11]. Huang et al. reported the formation of a localized high shear strain band in a plate sample under simple shear [15]. The shear band is in parallel configuration with the shear (as expected for a Lüders band) but did not across the entire gauge width of the sample (thus to form a band) and the global stress-strain response showed no strain softening but a monotonic hardening behaviour. Lüders-type deformation behaviour also did not happen in this case. However, torsion testing of thin wall tubes provides a practical case of shear with high "gauge length". Many studies have demonstrated the absence of Lüder-type deformation in such samples. Reedlunn et al. [16] conducted a complete tension-compression-torsion test of thin wall tube samples, following an earlier work by Sun and Li [13]. Both works demonstrate clearly the formation of a Lüders band under tension and the disappearance of the Lüders band when shear deformation becomes dominant. This also suggests that absence of Lüders-type deformation in shear cannot be argued for the lack of sufficient sample gauge length.

Another interesting case is stress-induced martensitic transformation of NiTi in bending mode [12, 50, 51]. Watkins et al. conducted a four-point bending test of pseudoelastic NiTi rod and thin wall tube samples [50]. The rod sample exhibited a unique deformation localization behaviour, with enhanced strains in the outer layers on both the tensile side and the compressive side. Such behaviour is different from the typical Lüders-type deformation expected, apparently due to the self-constraint between the higher strained surface and lower strained core regions in bending, preventing the "free" Lüders-type deformation. The tube sample, due to the emptiness underneath the tube wall along the bending axis and thus the absence of self-constraint to deformation, is more comparable to uniaxial tensile and compressive tests. This sample exhibited a Lüders-type localized deformation on the tensile side and uniform deformation on the compression side. The compressive side can be effectively considered a test of compression with a long gauge length. Thus, this test provides another evidence of the absence of Lüders deformation in compression with long gauge length, echoing Orgéas and Favier's work discussed above [11].

The evidence discussed above demonstrates that the absence of Lüders-type deformation in compression and in shear cannot be explained by the lack of sufficient gauge length for elastic contraction, but by other reasons, for example metallurgical, texture or crystallographic reasons. In fact, the suppression of Lüders-type deformation by such factors is also evident in the literature. One example is the "linear pseudoelastic behaviour" (total absence of Lüders deformation) of cold worked [52-54] or pseudoelastically cycled NiTi under tension [55, 56]. This may be attributed to the effect of massive defects within the matrix introduced by the processes. In another work by Grassi et al [57], a flattened Ti-50.8at%Ni sheet of a thin wall tube was used to fabricate tensile samples at various orientations from 0° to 90° relative to the tube axial direction. They found that whereas samples oriented in both the longitudinal (at 0°~22.5°) and the transverse (at 67.5°~90°) directions exhibited perfect pseudoelasticity in Lüders deformation mode, the 45°-oriented sample showed a perfect pseudoelasticity in the total absence of Lüders deformation behaviour. This experiment gives direct evidence to the effect of metallographic texture.

To put this into the context of this model, considering that the sample elongation change conservation criterion expressed in Eq. (2) is non-negotiable, it implies that the demand for elastic strain contraction is negligible or nil for compression, shear or in the cases of heavily

defected matrices and certain metallographic textures. This could be a result of $\dot{\varepsilon}_L$ being small so that $\dot{\delta}_L = \dot{\delta}_M$. This, obviously, is subjective to future experimental verification. In this regard, Eq. (2) is a necessary condition for Lüders-type deformation of NiTi, but not a sufficient condition.

6,2 Lüders band deformation via martensite reorientation

Lüders band behaviour is also observed for tensile deformation via martensite reorientation of polycrystalline NiTi [5]. The model presented above is also fully valid in this case. This may be explained in two aspects. First, the model is built purely on the consideration of the mechanical behaviour, with no reference to a phase transformation or otherwise. Second, the mechanical behaviour is characterized by two distinctive features, i.e., that the strain change across the Lüders band interface is a finite-discrete value and that the occurrence of this discrete strain change is intrinsically very fast (at the speed of sound in the medium) in the local scene. The macroscopic strain of stress-induced martensite reorientation is essentially the same as that of the stress-induced martensitic transformation, because they both are the manifestation of the same transformation crystallographic lattice distortion. The fast speed of propagation of the transformation interface is out of the need to accommodate such large crystallographic lattice distortions (as explained in section 3.1). Such need is also the same for martensite reorientation and for stress-induced martensitic transformation.

7. Conclusions

This study proposed a new explanation for the occurrence of the Lüders-type deformation of stress-induced martensitic transformation in polycrystalline NiTi. The explanation is based on the criterion of real-time conservation of sample dimension changes from three contributions, including the dimension change applied by the testing machine, the dimension change produced by the Lüders band formation or expansion, and the elastic strain contraction of the sample. Based on this criterion and the experimental evidence presented, the following conclusions are reached:

(1) The Lüders band of the stress-induced martensitic transformation of polycrystalline NiTi initiates suddenly within a finite width and a high local strain rate that can be orders of magnitude higher than the applied strain rate in a typical tensile testing. This leads to a sample elongation rate faster than the applied elongation rate by the testing machine. This causes an elastic strain contraction of the sample to produce a negative elongation to

compensate for the elongation shortfall provided by the testing machine. The elastic strain contraction causes the stress drop marking the initiation of the Lüders band.

(2) Based on the criterion of real-time sample elongation conservation, a mathematical model with experimental input is established. This model is able to describe the full stress-strain response of the Lüders-type deformation of NiTi, including the initial stress drop and strain reduction, and the stress plateau that follows. The reproduced behaviour matches perfectly with the experimental measurement. According to this criterion, the initial "upper-lower yielding behaviour of the Lüders-type deformation is defined by the condition that the rate of sample elongation from the Lüders band is higher than that from the testing machine, i.e., $\dot{\delta}_L > \dot{\delta}_M$, whereas the stress plateau section is defined by $\dot{\delta}_L = \dot{\delta}_M$.

(3) The sample elongation conservation-based model describes a necessary condition for the occurrence of the Lüders-type deformation, but not a sufficient condition. Other factors may take effect to prevent the Lüders-type deformation behaviour, e.g., metallographic and crystallographic textures, high density of defects, and compression and shear.

(4) Considering that the criterion is a necessary condition for Lüders-type deformation, the absence of Lüders-type deformation in compression (including solid bending) or shear (including torsion) suggests that in these deformation modes the rate of sample dimension change produced by the stress-induced martensitic transformation is slow and conforms to $\dot{\delta}_L = \dot{\delta}_M$, so that no elastic strain contraction ($\dot{\delta}_{el} = 0$) is required for sample dimension change compensation. This is a logical deduction from the criterion, and it obviously requires experimental verification, e.g., by DIC analysis.

(5) It is also worth noting, though not directly verified in this study, that the criterion and the model proposed above are equally valid for the case of Lüders-type deformation via martensite reorientation of NiTi, given that the model is built solely on mechanical considerations without any reference to a phase transformation and that the mechanical characteristics of deformation via martensite reorientation are practically identical to those via stress-induced martensitic transformation.

Acknowledgement

The authors wish to acknowledge the financial support from the Australian Research Council in grants DP180101955 and DP190102990 for this study. YW acknowledges the support from the US National Science Foundation under Grant DMR-1923929, which has facilitated this

international collaboration.

Reference

[1] J.A. Shaw, S. Kyriakides, On the nucleation and propagation of phase transformation fronts in a NiTi alloy, Acta materialia 45(2) (1997) 683-700.
[2] S. Miyazaki, T. Imai, K. Otsuka, Y. Suzuki, Lüders-like deformation observed in the transformation pseudoelasticity of a Ti-Ni alloy, Scripta Metallurgica 15(8) (1981) 853-856.
[3] E.O. Hall, Yield point phenomena in metals and alloys, Springer Science & Business Media2012.
[4] G. Tan, Y. Liu, P. Sittner, M. Saunders, Lüders-like deformation associated with stress-induced martensitic transformation in NiTi, Scripta Materialia 50 (2004) 193-198.
[5] Y. Liu, Y. Liu, J. Humbeeck, Lüders-like deformation associated with martensite reorientation in NiTi, Scripta materialia 39 (1998) 1047-1055.
[6] P. Sittner, Y. Liu, V. Novák, On the origin of Lüders-like deformation of NiTi shape memory alloys, Journal of the Mechanics and Physics of Solids 53(8) (2005) 1719-1746.
[7] C. Efstathiou, H. Sehitoglu, J. Carroll, J. Lambros, H. Maier, Full-field strain evolution during intermartensitic transformations in single-crystal NiFeGa, Acta Materialia 56(15) (2008) 3791-3799.
[8] F. de Castro Bubani, M. Sade, F. Lovey, Improvements in the mechanical properties of the 18R↔ 6R high-hysteresis martensitic transformation by nanoprecipitates in CuZnAl alloys, Materials Science and Engineering: A 543 (2012) 88-95.
[9] J. Yaacoub, Y. Wu, W. Abuzaid, D. Canadinc, H. Sehitoglu, Martensite variant localization effects on fatigue crack growth-The CuZnAl example, Scripta Materialia 171 (2019) 112-117.
[10] R. Sidharth, Y. Wu, F. Brenne, W. Abuzaid, H. Sehitoglu, Relationship between functional fatigue and structural fatigue of iron-based shape memory alloy FeMnNiAl, Shape Memory and Superelasticity 6 (2020) 256-272.
[11] L. Orgéas, D. Favier, Stress-induced martensitic transformation of a NiTi alloy in isothermal shear, tension and compression, Acta Materialia 46(15) (1998) 5579-5591.
[12] B. Reedlunn, C.B. Churchill, E.E. Nelson, J.A. Shaw, S.H. Daly, Tension, compression, and bending of superelastic shape memory alloy tubes, Journal of the Mechanics and Physics of Solids 63 (2014) 506-537.
[13] Q.-P. Sun, Z.-Q. Li, Phase transformation in superelastic NiTi polycrystalline micro-tubes under tension and torsion—from localization to homogeneous deformation, International Journal of Solids and Structures 39(13-14) (2002) 3797-3809.
[14] V. Grolleau, H. Louche, V. Delobelle, A. Penin, G. Rio, Y. Liu, D. Favier, Assessment of tension–compression asymmetry of NiTi using circular bulge testing of thin plates, Scripta materialia 65 (2011) 347-350.
[15] H. Huang, B. Durand, Q.P. Sun, H. Zhao, An experimental study of NiTi alloy under shear loading over a large range of strain rates, International Journal of Impact Engineering 108 (2017) 402-413.
[16] B. Reedlunn, W.S. LePage, S.H. Daly, J.A. Shaw, Axial-torsion behavior of superelastic tubes: Part I, proportional isothermal experiments, International Journal of Solids and Structures 199 (2020) 1-35.
[17] P. Sedlák, M. Frost, M. Ševčík, H. Seiner, 3D spatial reconstruction of macroscopic austenite–martensite transition zones in NiTi wires induced by tension and twisting using diffraction/scattering computed tomography, International Journal of Solids and Structures 228 (2021) 111122.
[18] Z. Li, Q. Sun, The initiation and growth of macroscopic martensite band in nano-grained

NiTi microtube under tension, International Journal of plasticity 18(11) (2002) 1481-1498.
[19] P. Feng, Q. Sun, Experimental investigation on macroscopic domain formation and evolution in polycrystalline NiTi microtubing under mechanical force, Journal of the Mechanics and Physics of Solids 54(8) (2006) 1568-1603.
[20] J.A. Shaw, S. Kyriakides, Initiation and propagation of localized deformation in elasto-plastic strips under uniaxial tension, International journal of plasticity 13(10) (1997) 837-871.
[21] B.S. Shariat, S. Bakhtiari, H. Yang, Y. Liu, Computational and experimental analyses of martensitic transformation propagation in shape memory alloys, Journal of Alloys and Compounds 806 (2019) 1522-1528.
[22] B.S. Shariat, S. Bakhtiari, H. Yang, Y. Liu, Controlled initiation and propagation of stress-induced martensitic transformation in functionally graded NiTi, Journal of Alloys and Compounds 851 (2021) 156103.
[23] D. Favier, H. Louche, P. Schlosser, L. Orgéas, P. Vacher, L. Debove, Homogeneous and heterogeneous deformation mechanisms in an austenitic polycrystalline Ti–50.8 at.% Ni thin tube under tension. Investigation via temperature and strain fields measurements, Acta Materialia 55(16) (2007) 5310-5322.
[24] H. Louche, P. Schlosser, D. Favier, L. Orgéas, Heat source processing for localized deformation with non-constant thermal conductivity. Application to superelastic tensile tests of NiTi shape memory alloys, Experimental mechanics 52(9) (2012) 1313-1328.
[25] C. Elibol, M.F.-X. Wagner, Virtual Extensometer Analysis of Martensite Band Nucleation, Growth, and Strain Softening in Pseudoelastic NiTi Subjected to Different Load Cases, Materials 11(8) (2018) 1458.
[26] B.S. Shariat, Y. Li, H. Yang, Y. Wang, Y. Liu, On the Lüders band formation and propagation in NiTi shape memory alloys, Journal of Materials Science & Technology 116 (2022) 22-29.
[27] D. Delpueyo, A. Jury, X. Balandraud, M. Grédiac, Applying Full-Field Measurement Techniques for the Thermomechanical Characterization of Shape Memory Alloys: A Review and Classification, Shape Memory and Superelasticity 7 (2021) 1-29.
[28] F. Furgiuele, P. Magarò, C. Maletta, E. Sgambitterra, Functional and structural fatigue of pseudoelastic NiTi: global vs local thermo-mechanical response, Shape Memory and Superelasticity 6 (2020) 242-255.
[29] M. Young, M.-X. Wagner, J. Frenzel, W.W. Schmahl, G. Eggeler, Phase volume fractions and strain measurements in an ultrafine-grained NiTi shape-memory alloy during tensile loading, Acta Materialia 58(7) (2010) 2344-2354.
[30] X. Bian, A.A. Saleh, P.A. Lynch, C.H. Davies, E.V. Pereloma, A.A. Gazder, An in-situ synchrotron study of the B2→ B19′ phase transformation in a Ni-Ti alloy subjected to uniaxial monotonic tension, Materials Science and Engineering: A 743 (2019) 327-338.
[31] P. Gao, R. Li, Y. Liu, G. Chen, M. Zhu, Y. Jian, Z. Wu, X. Lu, Y. Ren, C. Li, In-situ synchrotron diffraction study of the localized phase transformation and deformation behavior in NiTi SMA, Materials Science and Engineering: A 805 (2021) 140560.
[32] P. Sedmák, J. Pilch, L. Heller, J. Kopeček, J. Wright, P. Sedlák, M. Frost, P. Šittner, Grain-resolved analysis of localized deformation in nickel-titanium wire under tensile load, Science 353 (2016) 559-562.
[33] P. Šittner, P. Lukáš, V. Novák, M. Daymond, G. Swallowe, In situ neutron diffraction studies of martensitic transformations in NiTi polycrystals under tension and compression stress, Materials Science and Engineering: A 378(1-2) (2004) 97-104.
[34] S. Mao, J. Luo, Z. Zhang, M. Wu, Y. Liu, X. Han, EBSD studies of the stress-induced B2–B19′ martensitic transformation in NiTi tubes under uniaxial tension and compression, Acta Materialia 58(9) (2010) 3357-3366.

[35] Y. Liu, Z. Xie, J.V. Humbeeck, L. Delaey, Y. Liu, On the deformation of the twinned domain in NiTi shape memory alloys, Philosophical Magazine A 80(8) (2000) 1935-1953.
[36] E. Corona, J.A. Shaw, M.A. Iadicola, Buckling of steel bars with Lüders bands, International journal of solids and structures 39(13-14) (2002) 3313-3336.
[37] A. Weidner, Deformation Processes in TRIP/TWIP Steels: In-situ Characterization Techniques, Springer Nature2020.
[38] Y. Liu, On the nucleation and propagation of stress-induced martensitic transformation in NiTi, Materials science & engineering. A, Structural materials: properties, microstructure and processing 271(1-2) (1999) 506-508.
[39] J.F. Hallai, S. Kyriakides, Underlying material response for Lüders-like instabilities, International Journal of Plasticity 47 (2013) 1-12.
[40] D. Jiang, S. Kyriakides, C.M. Landis, K. Kazinakis, Modeling of propagation of phase transformation fronts in NiTi under uniaxial tension, European Journal of Mechanics-A/Solids 64 (2017) 131-142.
[41] M. Frost, B. Benešová, H. Seiner, M. Kružík, P. Šittner, P. Sedlák, Thermomechanical model for NiTi-based shape memory alloys covering macroscopic localization of martensitic transformation, International Journal of Solids and Structures 221 (2021) 117-129.
[42] D. Jiang, S. Kyriakides, C.M. Landis, Propagation of phase transformation fronts in pseudoelastic NiTi tubes under uniaxial tension, Extreme Mechanics Letters 15 (2017) 113-121.
[43] M. Rezaee-Hajidehi, K. Tůma, S. Stupkiewicz, Gradient-enhanced thermomechanical 3D model for simulation of transformation patterns in pseudoelastic shape memory alloys, International Journal of Plasticity 128 (2020) 102589.
[44] L. Kaufmann, M. Cohen, Thermodynamics and Kinetics of Martensitic Transformation, Progr. Met. Phys 7 (1958) 165.
[45] R. Bunshah, R. Mehl, Rate of propagation of martensite, Transactions of the American Institute of Mining and Metallurgical Engineers 197(9) (1953) 1251-1258.
[46] K. Otsuka, X. Ren, Physical metallurgy of Ti–Ni-based shape memory alloys, Progress in materials science 50(5) (2005) 511-678.
[47] L. Delaey, Diffusionless transformations, Phase Transformations in Materials 1 (2001) 583-654.
[48] S. Miyazaki, K. Otsuka, C. Wayman, The shape memory mechanism associated with the martensitic transformation in Ti-Ni alloys—II. Variant coalescence and shape recovery, Acta metallurgica 37(7) (1989) 1885-1890.
[49] T. Alonso, D. Favier, G. Chagnon, Characterizing transformation phenomena and elastic moduli of austenite and oriented martensite of superelastic thin NiTi wire through isothermal dynamic mechanical analysis, Journal of Materials Engineering and Performance 28 (2019) 4667-4679.
[50] R.T. Watkins, B. Reedlunn, S. Daly, J.A. Shaw, Uniaxial, pure bending, and column buckling experiments on superelastic NiTi rods and tubes, International Journal of Solids and Structures 146 (2018) 1-28.
[51] D. Jiang, S. Kyriakides, N.J. Bechle, C.M. Landis, Bending of pseudoelastic NiTi tubes, International Journal of Solids and Structures 124 (2017) 192-214.
[52] Y. Zheng, B. Huang, J. Zhang, L. Zhao, The microstructure and linear superelasticity of cold-drawn TiNi alloy, Materials Science and Engineering: A 279(1-2) (2000) 25-35.
[53] V. Delobelle, G. Chagnon, D. Favier, T. Alonso, Study of electropulse heat treatment of cold worked NiTi wire: From uniform to localised tensile behaviour, Journal of Materials Processing Technology 227 (2016) 244-250.
[54] H.M.R. de Oliveira, H. Louche, E.N.D. Grassi, D. Favier, Specific forward/reverse latent heat and martensite fraction measurement during superelastic deformation of nanostructured

NiTi wires, Materials Science and Engineering: A 774 (2020) 138928.
[55] Y. Liu, I. Houver, H. Xiang, L. Bataillard, S. Miyazaki, Strain dependence of pseudoelastic hysteresis of NiTi, Metallurgical and Materials Transactions A 30(5) (1999) 1275-1282.
[56] S. Zhao, Q. Liang, C. Liang, D. Wang, Y. Ji, Y. Wang, Y. Zheng, X. Ding, M. Mills, X. Ren, Quasi- Linear Superelasticity with Ultralow Modulus in Tensile Cyclic Deformed TiNi Strain Glass, Advanced Engineering Materials (2022) 2200239.
[57] E.N.D. Grassi, G. Chagnon, H.M.R. de Oliveira, D. Favier, Anisotropy and Clausius-Clapeyron relation for forward and reverse stress-induced martensitic transformations in polycrystalline NiTi thin walled tubes, Mechanics of Materials 146 (2020) 103392.